

Bias-Aware BP Decoding of Quantum Codes via Directional Degeneracy

Mohammad Rowshan
 University of New South Wales (UNSW)
 Sydney, Australia
 Email: mrowshan@ieee.org

Abstract—We study *directionally informed belief propagation (BP) decoding* for quantum CSS codes, where anisotropic Tanner-graph structure and biased noise concentrate degeneracy along preferred directions. We formalize this by placing orientation weights on Tanner-graph edges, aggregating them into per-qubit directional weights, and defining a *directional degeneracy enumerator* that summarizes how degeneracy concentrates along those directions. A single bias parameter β maps these weights into site-dependent log-likelihood ratios (LLRs), yielding anisotropic priors that plug directly into standard BP→OSD decoders without changing the code construction. We derive bounds relating directional and Hamming distances, upper bound the number of degenerate error classes per syndrome as a function of distance, rate, and directional bias, and give a MacWilliams-type expression for the directional enumerator. Finite-length simulations under code-capacity noise show significant logical error-rate reductions—often an order of magnitude at moderate physical error rates—confirming that modest anisotropy is a simple and effective route to hardware-aware decoding gains.

I. INTRODUCTION

Quantum LDPC (qLDPC) codes combine sparse parity checks with families of constant rate and linear (or near-linear) distance [1]–[6]. Lifted-product codes [4] and quantum Tanner codes [5] provide asymptotically good families with efficient decoders, yet practical decoding at finite blocklength is complicated by short cycles and *degeneracy*, the fact that many distinct errors share a syndrome and act identically on the codespace [7], [8].

Physical noise processes are typically anisotropic: dephasing errors can dominate bit flips and mixed errors, and hardware layouts often favor certain coupling directions. Bias-tailored surface codes and related CSS constructions show that aligning stabilizers and decoders with such bias can produce significant threshold and overhead improvements [9]–[11]. Most of this literature either changes the *code* to match a given biased channel, or uses decoders whose priors do not explicitly encode directional structure in the Tanner graph.

This work focuses on the decoder side and keeps the code fixed. We annotate the Tanner graphs of a CSS code with directional edge weights that reflect layout, scheduling, or calibrated anisotropy. Summing these edge weights gives per-qubit directional weights and a weighted Hamming cost, which in turn define a directional degeneracy enumerator. A single parameter β converts these directional weights into site-dependent LLRs for a standard BP→OSD decoder. The

same β controls a family of partition functions that count and reweight degenerate error classes, yielding both analytical insight and a practical tuning knob.

At a high level, the contributions are as follows. First, we introduce directional edge weights and the resulting per-qubit weights, and use them to define a directional degeneracy metric and enumerator. Second, we derive bounds that compare directional and Hamming distances, and prove a directionality-induced degeneracy bound that makes explicit how directional bias reduces the number of degenerate error classes per syndrome. Third, we present an anisotropic BP+OSD decoder that uses the directional weights through a single bias parameter, and we show through finite-length simulations that this anisotropy yields substantial logical error-rate reductions without altering the underlying code.

II. NOTATIONS AND PRELIMINARIES

We consider CSS stabilizer codes specified by binary parity-check matrices

$$H_X \in \mathbb{F}_2^{m_X \times n}, \quad H_Z \in \mathbb{F}_2^{m_Z \times n},$$

satisfying the commutation condition $H_X H_Z^\top = 0$. Their row spaces

$$S_X := \text{rowsp}(H_X), \quad S_Z := \text{rowsp}(H_Z)$$

encode the supports of X - and Z -stabilizer generators. Associated classical codes are

$$C_X := \ker(H_X), \quad C_Z := \ker(H_Z),$$

with $C_Z \subseteq C_X^\perp$ and $C_X \subseteq C_Z^\perp$ under the standard inner product. The number of logical qubits is

$$k = n - \text{rank}(H_X) - \text{rank}(H_Z).$$

Throughout we use the CSS picture: X - and Z -errors are decoded separately. For a fixed Z -syndrome s_Z , let e_0 be a solution of $H_Z e = s_Z$. All solutions are of the form $e_0 + C_Z$. Two such solutions are indistinguishable if they differ by an X -stabilizer, i.e., if their difference lies in S_X .

Definition 1 (Degeneracy classes). *For a fixed Z -syndrome s_Z , the set of degenerate error classes is the quotient*

$$\mathcal{D}_X(s_Z) \cong (e_0 + C_Z)/S_X. \quad (1)$$

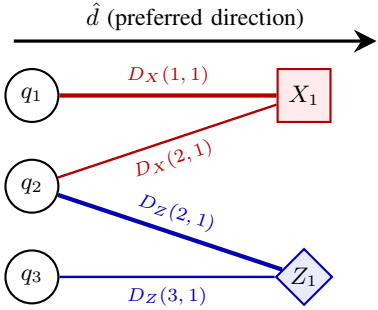


Fig. 1. Directionally annotated Tanner graph. Edge thickness encodes the magnitude of orientation weights D_X, D_Z . Summing over incident edges yields per-qubit directional weights w_i that define the cost $\Delta_w(E)$.

Its size is $|\mathcal{D}_X(s_Z)| = 2^k$ and does not depend on the syndrome.

An analogous definition applies on the Z side for X -syndromes. The objects in $\mathcal{D}_X(s_Z)$ index distinct logical X -actions compatible with the observed Z -syndrome. The directional framework developed below reweights these classes based on their alignment with a preferred direction.

III. DIRECTIONAL WEIGHTS AND DEGENERACY ENUMERATOR

A. Directional annotation of the Tanner graph

We view the CSS code through its Tanner graphs. For qubit i , let $N_X(i)$ be the set of adjacent X -checks and $N_Z(i)$ the set of adjacent Z -checks in bipartite graphs of H_X and H_Z .

Definition 2 (Directional annotation). A directionally annotated CSS code consists of (H_X, H_Z) together with nonnegative edge weight matrices

$$D_X \in \mathbb{R}_{\geq 0}^{n \times m_X}, \quad D_Z \in \mathbb{R}_{\geq 0}^{n \times m_Z},$$

supported on the edges of the X - and Z -Tanner graphs, respectively. A larger entry $D_X(i, j)$ or $D_Z(i, j)$ indicates that qubit i couples more strongly to check j along a preferred direction, for instance due to geometry, scheduling, or hardware-specific anisotropy (e.g., specific behavior of noise).

Summing the edge weights incident to qubit i produces a per-qubit directional weight

$$w_i := \sum_{j \in N_X(i)} D_X(i, j) + \sum_{j \in N_Z(i)} D_Z(i, j), \quad \mathbf{w} = (w_1, \dots, w_n). \quad (2)$$

So w_i says: how strongly qubit i is involved in “directionally important” edges overall. For a binary error indicator $E \in \{0, 1\}^n$, the corresponding directional cost is then

$$\Delta_w(E) = \sum_{i=1}^n w_i E_i = \langle \mathbf{w}, E \rangle. \quad (3)$$

That’s just a weighted Hamming weight: each flipped qubit i contributes w_i instead of “1”. Errors on “directionally important” qubits are thus counted as more expensive.

Figure 1 shows a toy Tanner graph with edge weights. In practice, the entries of D_X, D_Z can be derived from geometry, readout and gate scheduling, or from hardware calibration data, but the theory below requires only that they be nonnegative.

Proposition 1 (Edge-to-qubit reduction). *For an error indicator $E \in \{0, 1\}^n$, define*

$$\Delta_D(E) := \sum_{i: E_i=1} w_i,$$

that is, the sum of directional edge weights incident on the support of E . Then, $\Delta_D(E) = \Delta_w(E)$ with w_i given by (2).

Proof. Using $E_i \in \{0, 1\}$, $\Delta_D(E) = \sum_{i=1}^n w_i E_i = \Delta_w(E)$. \square

Thus, the directional annotation can be reduced to a per-qubit vector \mathbf{w} and a linear functional Δ_w , which are the only ingredients used in the enumerator and in the decoder.

B. Class scores and directional enumerator

For a fixed Z -syndrome s_Z , we have grouped all compatible X -errors into degeneracy classes $\mathcal{D}_X(s_Z)$. In decoding, we ultimately choose between *classes*, not individual representatives, so we need a single “directional cost” for each class built from Δ_w . Because Δ_w is not invariant under adding stabilizers, classes require their own scores.

Definition 3 (Class score). *For a fixed Z -syndrome s_Z and a class $[e] \in \mathcal{D}_X(s_Z)$, the class score is*

$$\Delta_*([e]) := \min_{u \in S_X} \Delta_w(e + u), \quad (4)$$

which is the cost of the least-cost representative, or weighted coset leader.

Definition 4 (Directional degeneracy enumerator). *For a fixed Z -syndrome s_Z and weights \mathbf{w} , the directional degeneracy enumerator is*

$$\Gamma_X(s_Z; \beta) := \sum_{[e] \in \mathcal{D}_X(s_Z)} \exp(-\beta \Delta_*([e])), \quad \beta \geq 0. \quad (5)$$

At $\beta = 0$ the enumerator equals 2^k ; its first derivative gives the mean class score and its second derivative the score variance. For $\beta > 0$, $\Gamma_X(s_Z; \beta)$ is dominated by classes with small $\Delta_*([e])$, and its decay in β measures how many such low-cost classes exist: fast decay means few, slow decay many. Thus Γ_X compactly summarizes how degeneracy distributes across directions under the per-qubit penalties \mathbf{w} .

Lemma 1 (Tail bound for low-cost classes). *Let $M_{\leq t}$ be the number of classes with $\Delta_*([e]) \leq t$. For any $\beta > 0$ and $t > 0$,*

$$M_{\leq t} \leq e^{\beta t} \Gamma_X(s_Z; \beta).$$

Proof. Restricting the sum in (5) to classes with cost at most t yields $\Gamma_X(s_Z; \beta) \geq M_{\leq t} e^{-\beta t}$. \square

Lemma 1 shows that, for fixed β , a small enumerator forces the number of low-cost classes to be small. Directional

weighting thus provides a handle for thinning out competitive low-cost classes, which is what we want for decoding: with fewer nearly equivalent low-cost options, the decoder has fewer opportunities to confuse logical errors.

IV. ANALYTICAL PROPERTIES

The directional enumerator admits useful inequalities and dual representations. We first compare directional and Hamming distances and then give a MacWilliams-type form for a global enumerator.

A. Directional distances

Let d be the (Hamming) code distance and d_S the minimum Hamming weight among nontrivial stabilizers in $S_X \cup S_Z$. Let $w_{\min} = \min_i w_i$ and $w_{\max} = \max_i w_i$.

Proposition 2 (Comparison with Hamming distance). *Let d_w^S be the minimum directional cost among nontrivial stabilizers and d_w^L the minimum directional cost among nontrivial logical operators. Then*

$$w_{\min} d_S \leq d_w^S \leq w_{\max} d_S, \quad w_{\min} d \leq d_w^L \leq w_{\max} d.$$

Proof. For any nonzero vector v , we have $w_{\min} \text{wt}(v) \leq \sum_i w_i v_i \leq w_{\max} \text{wt}(v)$. Applying this to the Hamming-minimizing stabilizers and logicals gives the claim. \square

Directional distances therefore inherit scaling from classical distances. Mild anisotropy ($w_{\min} \approx w_{\max}$) preserves distances up to a small factor; strong anisotropy can alter them significantly if logical and stabilizer supports are aligned with low- or high-weight directions.

B. Directionality-induced degeneracy bound

We bound how many degenerate error classes remain admissible once a directional model is imposed. Let $[\![n, k, d_{\min}]\!]$ be a CSS code with rate $R = k/n$ and minimum distance d_{\min} . Suppose the directional model filters classes according to an admissibility rule. For example, one may require that an admissible class contain a representative whose support lies mostly along the favored direction according to D_X .

For each syndrome s_Z , let $\mathcal{D}_\delta(s_Z) \subseteq \mathcal{D}_X(s_Z)$ be the subset of classes that are admissible under the directional model. Define the worst-case concentration factor

$$f(\delta_{\max}, R) := \sup_{s_Z} \frac{|\mathcal{D}_\delta(s_Z)|}{|\mathcal{D}_X(s_Z)|},$$

where $\delta_{\max} \geq 0$ is any scalar that summarizes the maximum directional bias, for instance $\delta_{\max} = \max_{i,j} D_X(i, j)$. Since directionality only removes classes, $f(\delta_{\max}, R) \leq 1$ and $f(0, R) = 1$.

Lemma 2 (Directionality-induced degeneracy bound). *For every syndrome s_Z ,*

$$|\mathcal{D}_\delta(s_Z)| \leq 2^k f(\delta_{\max}, R) \leq 2^{n-2d_{\min}+2} f(\delta_{\max}, R).$$

Proof. The isotropic degeneracy count is $|\mathcal{D}_X(s_Z)| = 2^k$; admissibility only removes classes, giving $|\mathcal{D}_\delta(s_Z)| \leq$

$2^k f(\delta_{\max}, R)$. The quantum Singleton bound [12] implies $k \leq n - 2d_{\min} + 2$, hence $2^k \leq 2^{n-2d_{\min}+2}$. \square

Lemma 2 makes explicit how directional structure can reduce the effective degeneracy of the code. The concentration factor $f(\delta_{\max}, R)$ depends on the directional rule and on the code family; it is monotone nonincreasing in the strength of the bias. In examples where directional structure correlates with logical operators, one expects $f(\delta_{\max}, R)$ to be significantly smaller than 1 for moderate δ_{\max} .

C. Global enumerator and MacWilliams representation

Let $C := C_X \cap C_Z$ and consider the global directional enumerator

$$\Gamma(\mathbf{w}; \alpha) := \sum_{v \in C} e^{\alpha \langle \mathbf{w}, v \rangle}, \quad \alpha > 0. \quad (6)$$

This is the specialization at $(x_i, y_i) = (1, e^{\alpha w_i})$ of the per-coordinate complete weight enumerator

$$W_C(\{x_i, y_i\}_{i=1}^n) := \sum_{v \in C} \prod_{i=1}^n x_i^{1-v_i} y_i^{v_i}.$$

Theorem 1 (MacWilliams-type specialization). *Let C^\perp be the dual of C under the standard inner product. Then*

$$\Gamma(\mathbf{w}; \alpha) = W_C(\{1, e^{\alpha w_i}\}) = \frac{1}{|C^\perp|} \sum_{u \in C^\perp} \prod_{i=1}^n (1 + (-1)^{u_i} e^{\alpha w_i}).$$

Proof. The first equality is the specialization $x_i = 1$, $y_i = e^{\alpha w_i}$. The second is the MacWilliams identity for the complete weight enumerator over \mathbb{F}_2 [13], which is a discrete Fourier transform on $\{0, 1\}^n$. \square

Theorem 1 connects directional degeneracy to the dual code and shows that the dependence on \mathbf{w} factorizes over coordinates in the dual domain. This form is useful when C^\perp has a structured description, such as in hypergraph-product or Tanner constructions.

The logarithm of Γ has convenient calculus identities. Writing $\pi_{\alpha, \mathbf{w}}(v) \propto e^{\alpha \langle \mathbf{w}, v \rangle}$ for the Gibbs distribution on C , we have

$$\frac{\partial}{\partial w_i} \log \Gamma(\mathbf{w}; \alpha) = \alpha \mathbb{E}_{\pi_{\alpha, \mathbf{w}}}[v_i]. \quad (7)$$

Thus increasing w_i suppresses coordinates with large expected occupancy. The function $\log \Gamma(\mathbf{w}; \alpha)$ is convex in \mathbf{w} since it is the log of a sum of exponentials of linear forms. Small ℓ_∞ perturbations of \mathbf{w} change $\log \Gamma$ by at most $O(\alpha n \|\delta\|_\infty)$; a simple argument using $|\langle \delta, v \rangle| \leq n \|\delta\|_\infty$ and bounding the ratio of exponentials yields a global Lipschitz constant.

V. ANISOTROPIC DECODING

We now describe how the directional weights are used in a practical BP+OSD decoder. The underlying code is unchanged; only the prior and the scoring function are modified.

A. Site-dependent priors from directional weights

Consider a memoryless binary-input channel (for one CSS side) with independent error probabilities p_i on each qubit. Under independence, the negative log-likelihood of an error pattern $E \in \{0, 1\}^n$ is

$$-\log \Pr(E) = \sum_i E_i \log \frac{p_i}{1-p_i} + \text{const} = \sum_i w_i^{\text{MAP}} E_i + \text{const},$$

with $w_i^{\text{MAP}} = \log \frac{1-p_i}{p_i}$. Thus, MAP decoding corresponds to weighted min-sum with weights w_i^{MAP} .

The directional weights \mathbf{w} from (2) provide a natural way to parametrize p_i . A convenient one-parameter family is

$$p_i(\beta) = \frac{p_0 e^{\beta w_i}}{\frac{1}{n} \sum_{j=1}^n e^{\beta w_j}}, \quad \ell_i(\beta) = \log \frac{1-p_i(\beta)}{p_i(\beta)}, \quad (8)$$

where p_0 is a target average physical error rate and $\beta \geq 0$ is a directional strength parameter. For $\beta = 0$ this reduces to the isotropic prior $p_i = p_0$. Increasing β makes errors more likely on qubits with larger w_i .

The LLRs $\ell_i(\beta)$ are passed to a standard belief-propagation decoder on the Tanner graph of H_X or H_Z . From the channel perspective, (8) is an exponential tilt of a baseline isotropic distribution, and the same β also appears in the directional enumerator through the weights.

B. MAP on trees and coset posteriors

When the factor graph of H is cycle-free, belief propagation is exact.

Theorem 2 (MAP on trees equals weighted min-sum). *Let $H \in \{0, 1\}^{m \times n}$ be a parity-check matrix whose factor graph is a forest. Suppose the physical noise on each qubit is independent with error probabilities $p_i \in (0, 1/2)$ and define*

$$w_i := \log \frac{1-p_i}{p_i}.$$

For a given syndrome s , let $\mathcal{S}(s) := \{E \in \{0, 1\}^n : HE = s\}$ be the affine solution set. If each syndrome s identifies a unique coset in $\mathcal{S}(s)$ (so that the MAP solution is unique up to stabilizers), then the MAP estimate

$$E^* \in \arg \max_{E \in \mathcal{S}(s)} \Pr(E \mid s)$$

coincides with

$$E^* = \arg \min_{E \in \mathcal{S}(s)} \sum_{i=1}^n w_i E_i,$$

and min-sum belief propagation on the factor graph of H with unary costs w_i returns E^ .*

On loopy graphs, BP is approximate, but the structure of coset posteriors remains clear.

Proposition 3 (Coset posterior). *For independent noise with probabilities p_i and weights w_i , the posterior probability of a coset $\mathcal{C} \subseteq \{E : HE = s\}$ given syndrome s satisfies*

$$\Pr(\mathcal{C} \mid s) \propto \sum_{v \in \mathcal{C}} \exp \left(- \sum_{i=1}^n w_i v_i \right).$$

Proof. Conditioning on $HE = s$ does not change the relative likelihoods within the solution set. The likelihood of v is proportional to $\exp(-\sum_i w_i v_i)$; the posterior of the coset is obtained by summing over its representatives. \square

Thus, degeneracy enters through a multiplicity-weighted partition function on each coset, controlled by w_i . Changing β in (8) modifies these partition functions and shifts which cosets have highest posterior mass.

C. Anisotropic BP+OSD decoder

In practice, we decode each CSS side as follows. The directional model provides D_X, D_Z and per-qubit weights \mathbf{w} . For a given physical error rate p_0 and bias parameter β , we form $p_i(\beta)$ and LLRs $\ell_i(\beta)$ from (8). These LLRs initialize a min-sum BP decoder, which is run for a number of iterations, and the tentative estimate is further refined by ordered-statistics decoding (OSD) of moderate order [8]. The same directional weights are used to rank candidates and break ties: among syndrome-consistent patterns, the decoder prefers smaller values of $\Delta_{\mathbf{w}}(E)$. The key point is that the code, the Tanner graph, and the OSD implementation are unchanged. The only difference between isotropic and anisotropic decoding is in how LLRs and candidate scores are computed from the directional weights and the scalar parameter β .

VI. NUMERICAL RESULTS

This section illustrates how anisotropic priors affect finite-length performance, via directional weights w_i and a scalar β . The same machinery can bias Tanner-graph edges in many other ways, e.g. stripwise piecewise-constant w_i for readout rows, checkerboard or layer-dependent weights modelling interleaved hardware sublattices, or radial gradients centred on a particularly noisy region of the device.

Note that anisotropic/directional priors are not a silver bullet: for codes whose degeneracy is essentially isotropic (e.g. ensemble-style qLDPCs with no meaningful geometric embedding) or for hardware where the noise is close to i.i.d., a one-dimensional anisotropic tilt may offer little or no benefit and can even degrade performance if the assumed orientation is badly misaligned with the true noise. More generally, when bias arises from complicated cross-qubit correlations rather than a smooth gradient (e.g. strongly gate- or chip-layout-dependent error patterns), richer hardware models are likely needed beyond the simple directional field considered here.

A. Orientation-based directional priors

We now specialise the directional framework of Section V (weights w_i , tilted probabilities $p_i(\beta)$, and LLRs $\ell_i(\beta)$) to two geometries: the planar [36, 4] NE3N code and the $[2L^2, 2, L]$ toric code ($L = 9$).

a) *NE3N planar code*.: The NE3N code [14] is realised on an 18×4 rectangular lattice with a bipartite data/ancilla layout, giving each physical qubit i integer coordinates $(x_i, y_i) \in \mathbb{Z}^2$. To model a horizontal hardware anisotropy (e.g. control lines running left-to-right), we choose the scalar coordinate

$$c_i := x_i \quad (9)$$

in the general construction of Section V, and obtain directional weights w_i by standardising $\{c_i\}$ across all data qubits, to obtain dimensionless directional weights

$$\bar{c} := \frac{1}{n} \sum_{i=1}^n c_i, \quad \sigma_c^2 := \frac{1}{n-1} \sum_{i=1}^n (c_i - \bar{c})^2, \quad (10)$$

$$w_i := \frac{c_i - \bar{c}}{\sigma_c}, \quad (11)$$

Qubits near the right edge then have $w_i > 0$, those near the left edge have $w_i < 0$, with a smooth gradient in between.

b) *Toric code*.: For the toric code, we consider an $L \times L$ square lattice with periodic boundary conditions, with one qubit on each horizontal and vertical edge. Horizontal edges are labelled

$$\text{idx}_h(x, y) = yL + x, \quad \text{coord}(\text{idx}_h(x, y)) = (2x, 2y),$$

and vertical edges

$$\text{idx}_v(x, y) = L^2 + yL + x, \quad \text{coord}(\text{idx}_v(x, y)) = (2x+1, 2y+1),$$

for $x, y \in \{0, \dots, L-1\}$ (with arithmetic modulo L). This embeds all $2L^2$ qubits at integer coordinates $(x_i, y_i) \in \{0, \dots, 2L-1\}^2$ on two interleaved checkerboard sublattices. To emulate a hardware gradient along one spatial axis, we again take $c_i := x_i$ and form w_i by standardising $\{c_i\}$ as before. Qubits at larger x -coordinate are thus “downstream” (positive w_i), and errors become more likely there as β increases.

c) *Alternative directional fields*.: The same mechanism can be used to define w_i in other hardware and code geometries. For example:

- *Vertical orientation*: set $c_i = y_i$ instead of x_i , so that directionality favours rows rather than columns.
- *Strip-wise weights*: choose a subset of “favoured” columns $\mathcal{C} \subset \{0, \dots, L_x-1\}$ and define $w_i = +w_0$ if $x_i \in \mathcal{C}$ and $w_i = -w_0$ otherwise, for some fixed contrast $w_0 > 0$.
- *Radial gradient*: for codes embedded in a disc or annulus, define c_i as the radial coordinate and apply the same standardisation and tilt as in (10)–(11) to favour qubits near or away from a boundary.

All of these choices are compatible with the directional enumerator and anisotropic decoding framework developed in Sections III and V; the only change is in how the per-qubit weights w_i are instantiated for a given code family and hardware noise model.

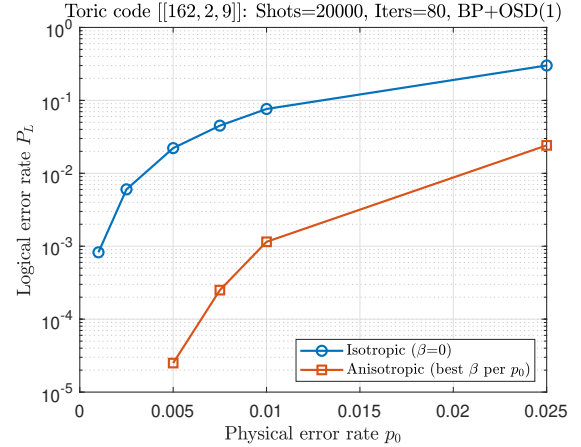


Fig. 2. Logical error rate vs. physical error rate for the $[[162, 2, 9]]$ Toric code

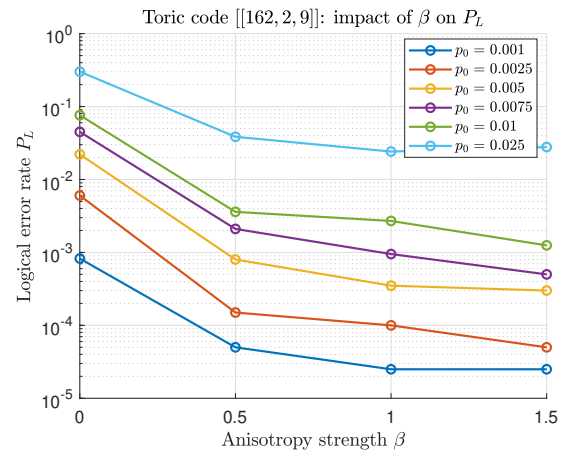


Fig. 3. P_L versus anisotropy strength β for the $[[162, 2, 9]]$ Toric code

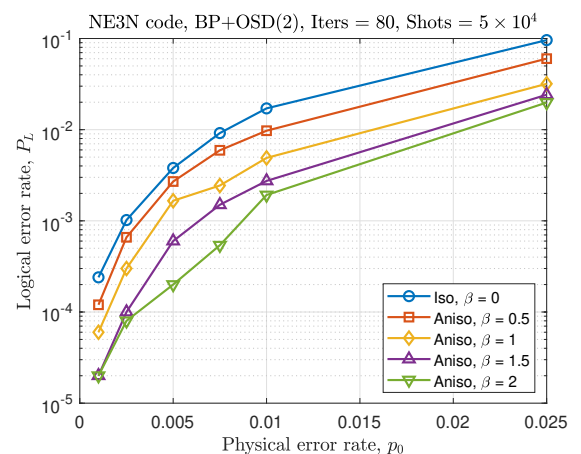


Fig. 4. Logical error rate vs. physical error rate for the $[36, 4]$ NE3N code

B. Logical error-rate behavior

Fig. 2 shows that across the range $p_0 \approx 10^{-3}$ – 10^{-2} , the directional prior, aligned with a geometric orientation of the toric lattice, reduces the logical error rate by roughly one to two orders of magnitude without modifying the code or the decoder architecture. Fig. 3 illustrates how the logical error rate varies with the anisotropy strength β , treating the isotropic decoder as the $\beta = 0$ baseline. The trend confirms that the parameter β provides an effective and tunable control for enhancing BP+OSD decoding performance. For the $[[36, 4]]$ NE3N code, Fig. 4 shows that orientation-based priors systematically outperform isotropic BP+OSD(2), reducing the logical error rate by roughly one order of magnitude across the tested physical error rates.

VII. CONCLUSION

We introduced a directional framework for quantum LDPC decoding that annotates Tanner graphs with orientation-aware edge weights, aggregates them into per-qubit directional weights, and feeds these into both a directional degeneracy enumerator and an anisotropic BP+OSD decoder. The theory relates directional and Hamming distances, bounds the number of degenerate error classes per syndrome in terms of rate, distance, and directional bias, and admits a MacWilliams-type representation of the enumerator, while finite-length simulations show that modest anisotropy, controlled by a single parameter β , can already yield substantial logical error-rate reductions without changing the code or decoder architecture. The framework is deliberately simple and portable: per-qubit weights can be derived from geometry and scheduling, then passed through the same LLR mapping and BP+OSD pipeline, and the same machinery can be layered on top of Pauli-biased noise by starting from different baseline X - and Z -error rates and applying the spatial tilt separately to each. Extending the numerics to the larger families of codes and scenarios, incorporating circuit-level and correlated noise, and using the enumerator’s gradient identities to learn directional priors from data are natural directions for further work.

REFERENCES

- [1] J. Tillich and G. Zémor, “Quantum ldpc codes with positive rate and minimum distance proportional to the square root of the blocklength,” *IEEE Transactions on Information Theory*, vol. 60, no. 2, pp. 1193–1202, 2014.
- [2] A. Leverrier, J. Tillich, and G. Zémor, “Quantum expander codes,” *2015 IEEE 56th Annual Symposium on Foundations of Computer Science (FOCS)*, pp. 810–824, 2015, see also arXiv:1504.00822.
- [3] S. Evra, T. Kaufman, and G. Zémor, “Decodable quantum ldpc codes beyond the \sqrt{n} distance barrier using high dimensional expanders,” *SIAM Journal on Computing*, vol. 51, no. 5, pp. 1436–1476, 2022, preprint: arXiv:2004.07935.
- [4] P. Panteleev and G. Kalachev, “Asymptotically good quantum and locally testable classical ldpc codes,” in *Proceedings of the 54th Annual ACM SIGACT Symposium on Theory of Computing (STOC)*, 2022, pp. 375–388, see also arXiv:2111.03654.
- [5] A. Leverrier and G. Zémor, “Quantum tanner codes,” *2022 IEEE 63rd Annual Symposium on Foundations of Computer Science (FOCS)*, pp. 872–883, 2022, see also arXiv:2202.13641.
- [6] N. P. Breuckmann and J. N. Eberhardt, “Quantum ldpc codes,” *PRX Quantum*, vol. 2, no. 4, p. 040101, 2021.
- [7] D. Poulin and Y. Chung, “On the iterative decoding of sparse quantum codes,” *Quantum Information & Computation*, vol. 8, no. 10, pp. 987–1000, 2008, arXiv:0801.1241.
- [8] P. Panteleev and G. Kalachev, “Degenerate quantum ldpc codes with good finite length performance,” *Quantum*, vol. 5, p. 585, 2021.
- [9] D. K. Tuckett, A. S. Darmawan, C. T. Chubb, S. Bravyi, S. D. Bartlett, and S. T. Flammia, “Tailoring surface codes for highly biased noise,” *Physical Review X*, vol. 9, no. 4, p. 041031, 2019.
- [10] J. P. Bonilla Ataides, D. K. Tuckett, S. D. Bartlett, S. T. Flammia, and B. J. Brown, “The xzzx surface code,” *Nature Communications*, vol. 12, no. 1, p. 217, 2021.
- [11] J. Roffe, L. Z. Cohen, A. O. Quintavalle, D. Chandra, and E. T. Campbell, “Bias-tailored quantum ldpc codes,” *Quantum*, vol. 7, p. 1005, 2023, see also arXiv:2202.01702.
- [12] E. Knill and R. Laflamme, “Theory of quantum error-correcting codes,” *Physical Review A*, vol. 55, no. 2, pp. 900–911, 1997.
- [13] E. M. Rains, “Quantum weight enumerators,” *IEEE Transactions on Information Theory*, vol. 44, no. 4, pp. 1388–1394, 1998, see also arXiv:quant-ph/9612015.
- [14] G. P. Gehér, D. Byfield, and A. Ruban, “Directional codes: a new family of quantum ldpc codes on hexagonal-and square-grid connectivity hardware,” *arXiv preprint arXiv:2507.19430*, 2025.
- [15] F. R. Kschischang, B. J. Frey, and H.-A. Loeliger, “Factor graphs and the sum-product algorithm,” *IEEE Transactions on information theory*, vol. 47, no. 2, pp. 498–519, 2002.

APPENDIX

PROOF OF THEOREM 2

Proof. Because errors are independent,

$$\Pr(E) = \prod_{i=1}^n p_i^{E_i} (1 - p_i)^{1 - E_i}.$$

The syndrome is a deterministic function $s = HE$, so $\Pr(s | E) = \mathbf{1}_{\{HE=s\}}$ and hence

$$\Pr(E | s) \propto \mathbf{1}_{\{HE=s\}} \Pr(E),$$

so maximizing $\Pr(E | s)$ over $\mathcal{S}(s)$ is equivalent to maximizing $\Pr(E)$ over $\mathcal{S}(s)$.

Taking minus the logarithm and discarding the additive constant that does not depend on E gives

$$-\log \Pr(E) = \sum_{i=1}^n E_i \log \frac{p_i}{1 - p_i} + \text{const} = \sum_{i=1}^n w_i E_i + \text{const},$$

with $w_i = \log \frac{1-p_i}{p_i}$. Thus

$$\arg \max_{E \in \mathcal{S}(s)} \Pr(E | s) = \arg \min_{E \in \mathcal{S}(s)} \sum_{i=1}^n w_i E_i,$$

which proves the weighted min-sum characterization of the MAP estimate.

To see that min-sum BP produces this minimizer, represent the posterior as a factor graph with variable nodes E_i and check nodes enforcing the parity constraints $H_a E = s_a$. The cost function is

$$F(E) = \sum_{i=1}^n w_i E_i + \sum_{a=1}^m \Psi_a(E_{N(a)}),$$

where Ψ_a is 0 if the parity at check a is satisfied and $+\infty$ otherwise. By assumption, the factor graph is a forest, i.e., a disjoint union of trees. On a tree factor graph, min-sum (equivalently, max-product in the log domain) belief propagation computes the exact global minimizer of any such additive, locally factored cost [15]. Applied to $F(E)$, min-sum BP therefore returns the unique minimizer in $\mathcal{S}(s)$, which is the MAP estimate E^* . \square